Effect of fluorinated additives or co-solvent on performances of graphite//LiMn2O4 cells cycled at high potential

Benjamin Flamme, Darius J. Yeadon, Satyajit Phadke, Mérièm Anouti

Effect of fluorinated additives or co-solvent on performances of graphite//$LiMn_2O_4$ cells cycled at high potential

Benjamin Flamme, Darius J. Yeadon, Satyajit Phadke, Mérièm Anouti*

Laboratoire PCM2E, EA 6299- Université de Tours, Faculté des Sciences et Techniques Parc de Grandmont, 37200 Tours, France

*Corresponding author.

E-mail address: meriem.anouti@univ-tours.fr (M. Anouti).

ABSTRACT

Herein, a comprehensive study of electrochemical performances of the combined effect of fluorinated additives; fluoroethylene carbonate (FEC); and tris(2,2,2-trifluoroethyl) phosphite (TTFP) or the 2,2,2-trifluoroethyl methyl carbonate (TFEMC) as co-solvent, on Graphite//$LiMn_2O_4$ cells cycled at high potential is reported. On one side, each additive has a specific function, the FEC is dedicated to the negative electrode and the TTFP to the opposite one. The electrolyte mixture with (4% FEC + 1% TTFP) additive has shown the best ability to reduce fading of the $LiMn_2O_4$ electrode, especially at high rates. On the other side, by studying the comparative thermal and transport properties of the formulated electrolytes with different proportions of TFEMC, we demonstrate that the difference in charge distribution of EMC and TFEMC molecules induced by the presence of fluorine atoms, modifies the solvation model of the Li^+ cation, and changes its behavior at the CEI interface and impact strongly the electrochemical performances. Finally, the EIS investigation of the LMO/electrolyte interfaces in the presence of TFEMC demonstrates that despite a spontaneous chemical reactivity of the TFEMC at the cathode interface over time, the conductive and good quality CEI is formed, which positively impact the cyclability. This study shows that against LMO surface phenomena, the combination in adequate proportions of fluorinated additives or solvent can be a solution not only to avoid the oxidative reactivity of LMO-cathode, but also to prevent its harmful consequences on the Li-metal or graphite-anode by controlling the solvation of lithium-ion.

***Keywords**:* Li-ion battery; LMO-cathode; Fluorinated-solvent; Additive; Fluoro-alkylcarbonate

1. Introduction

Lithium-ion batteries (LiBs) remain one of the most promising solutions to solve energy problems. LiBs have been studied and applied in many areas, such as: energy storage systems, portable electronic devices and electric vehicles [1-4]. Environmental considerations, as well as the shortage of some metals, tend to change battery components composition especially the positive electrode [5]. The spinel lithium manganese oxide ($LiMn_2O_4$) seems to be an interesting alternative to usual cathode materials, such as: lithium cobalt oxide ($LiCoO_2$) and lithium nickel cobalt manganese oxide types ($LiNi_xCo_yMn_zO_2$), due to its lower production cost, weak toxicity and high capacity [6-8]. Despite abundant and intensive studies in previous decades, $LiMn_2O_4$ continues to be penalized by a poor cycling stability, especially when graphite is used as negative electrode, and even more when temperature is increased [9-11].

The poor performances of $LiMn_2O_4$, in addition of common capacity fading caused by SEI and CEI (re)formations, are produced by multiple factors. Firstly, unstable structures are generated both at low and high state of charge. At low state of charge a Jahn-Teller distortion of Mn^{3+} cation takes place and leads to a structure modification [12]. It also allows a high disproportionation of Mn^{3+} into stable Mn^{4+} and soluble Mn^{2+} [13]. At a high state of charge, $LiMn_2O_4$ can insert extra lithium leading to a less stable phase [14]. Secondly, acid electrolytes which mainly consist of solvated HF, produced by hydrolysis of $LiPF_6$, dissolve manganese from the cathode and induce a direct loss of active material [8,10,11]. The generation of soluble Mn^{2+} cations produces a secondary negative effect on graphite electrode in case of full-cells. These cations are included into the SEI and enhance the continuous decomposition of the electrolyte [10,15]. Nevertheless, options exist to diminish the fading of $LiMn_2O_4$ cells with the use of additives, which have successfully demonstrated to appropriately passivate the electrode surface [11,16-19]. Another solution is to neutralize the

decomposition of $LiPF_6$ by removing traces of water and simultaneously reduce the acid dissolution of manganese into the electrolyte [20,21]. To find a solution we are focus on two pathways: (i) the action of additives to protect the interface and (ii) use a co-solvent as an agent to lower the electrolyte reactivity at the interface. In this study, we suggest focusing on fluorinated compounds (additives or co-solvents) to understand the beneficial action of fluorine on the electrolyte composition and consequently the electrochemical performances of Gr//LMO full-cells. These compounds have recently been highlighted again as valuable additives in both half and full-cells [22-25]. We propose in this work, in a first step the study, in Li//LMO half-cells then in Gr//LMO full-cells, of the combined effect of two fluorinated additives; the fluoroethylene carbonate (FEC); and the tris (2,2,2-trifluoroethyl) phosphite (TTFP). In a second step a study of the 2,2,2-trifluoroethylmethylcarbonate (TFEMC), a fluorinated co-solvent as an alternative to fluorinated additives, in Gr//LMO full-cells including its transport properties.

2. Experimental

2.1. Electrodes, electrolytes formulation and cell realizations

Commercial $LiMn_2O_4$ (TCI Deutschland GmbH) coated on Aluminum foil was employed in this study, with an active material loading of 85%. Positive electrodes were punched with a 10mm diameter for half-cells (typically 9 to 10 mg of active material) and 14 mm diameter for full-cells (16 to 19 mg of active material). Lithium anode (Sigma Aldrich, 99.9% 0.38 mm thickness) was used as counter electrode, and as a reference on a half-cell. Commercially available graphite coated on copper from SAFT (loading of 96.25%), was used as the anode on the full-cell. The graphite electrode was punched at 16 mm diameter to reach a 1.1 to 1.2 ratio between Graphite and LMO. CR-2032 type coin cells were assembled in an Argon filled glovebox (MBraun), two GF/C type Whatman glass microfiber filters with 16 mm diameters were soaked with 200 µL of electrolyte, and used as separators. All electrolyte formulations

are based on a mixture of 1.5 M lithium hexafluorophosphate, $LiPF_6$, salt (Sigma Aldrich, battery grade) and dissolved in ethylene carbonate, EC, (Sigma-Aldrich, battery grade) and ethyl methyl carbonate, EMC, (Merck chemicals, Selectilyte®) binary solvent mixture, with a mass ratio of 3 to 7 respectively, denoted (EC/EMC; 3/7, w/w). Other chemicals used were: (TFEMC, Apollo Scientific 99%); (FEC, Sigma-Aldrich 99%) and tris(2,2,2-trifluoroethyl) phosphite (TTFP, Sigma-Aldrich 99%). The electrolytes were prepared using a Sartorius 1602 MP balance with $\pm 10^{-4}$ g accuracy inside an argon filled MBraun glovebox, at 25 °C, with less than 5 ppm of moisture content. The water content of each electrolyte was measured using an 831 Karl-Fisher Coulometer (Metrohm), with values lower than 20 ppm.

2.2. Experimental

Conductivity measurements were performed using a BioLogic Multichannel conductivity Meter based on a frequency response Analyser (MCM 10) connected to a Peltier temperature-controlled unit with 10 slots (WTSH 10). The temperature was controlled by a JULABO thermostat bath with an accuracy of 0.2 °C, using sealed cells with parallel Pt plated electrodes, protecting the samples from exposure to air. The uncertainty of the conductivity measurements was better than 5.10^{-4} mS cm^{-1}.

Density and viscosity measurements were carried out at atmospheric pressure over a temperature range (283.15-333.15 K) on a U-shaped vibrating-tube densitometer (DMA 4500 M, Anton Parr, France) coupled with a rolling-ball microviscometer (Lovis 2000M/ME, Anton Parr, France). The internal calibration of the densitometer was confirmed by measuring densities of air and triple-distilled water (298.15 K), as recommended by the manufacturer, before every sample measurement, with an accuracy of 5.10^{-5} g cm^{-3}. The optimum angle for the microviscometer was automatically determined by the equipment, based on run time. Capillary tubes with nominal internal diameters of 1.59 and 1.80 mm,

previously calibrated as a function of temperature and angle of measurements with viscosity standards from the manufacturer, were used for measurements. The viscosity at each temperature was measured 10 times, with an estimated uncertainty 0.5%.

Electrochemical measurements were carried out at room temperature, galvanostatic cyclings were performed on a Biologic BCS-805 battery cycler or on a Biologic VMP-3 potentiostat between 3.2 V and 4.7 V for half-cells, and between 3.0 V and 4.7 V for full-cells unless otherwise stated. Electrochemical Impedance Spectroscopy (EIS) was performed on CR-2032 half-cells and recorded on Biologic VMP-3 over a range of frequencies, from 1 mHz to 1 MHz.

3. Results and discussion

3.1. The effect of fluorinated additives

The primary role of fluorinated electrolyte additives has concentrated on the formation of a robust and stable artificial solid-electrolyte interphase (SEI, CEI) on the electrodes. As is known, the HOMO and LUMO energies of the fluorinated molecules are lower than their non-fluorinated counterparts, due to the strong electron withdrawing ability of the fluorine, which is strongly electronegative [19,26]. Thus, oxidation potentials of fluorinated molecules are higher. In this study, FEC and the TTFP additives were firstly evaluated in half-cells as well as in Gr//LMO full-cells.

3.1.1. Half-cell systems and lithium metal surface role

Cyclic voltammetry (CV) and galvanostatic profiles under different cut-off potential from 4.3 to 4.8 V vs. Li^+/Li and of the baseline electrolyte ($LiPF_6$ 1.5 M in EC/EMC; 3/7, w/w) were performed on LMO//Li half-cells, and are shown in Fig. 1(a and b). The electrochemical process described by the reversible disproportionation reaction corresponds to the extraction

of x moles of lithium in two successive. The CVs (v = 50 µV s^{-1}) for Mn^{3+}/Mn^{2+} (P1) and Mn^{4+}/Mn^{3+} (P2) redox couples for octahedral-site manganese appear to be separated by about 200 mV (Fig. 1b). Goodenough *et al.* have reported that the reorganization energy is regained by changing the valence from high spin Mn^{3+} to Mn^{4+} in an octahedral site is 0.3-0.5 eV [27].

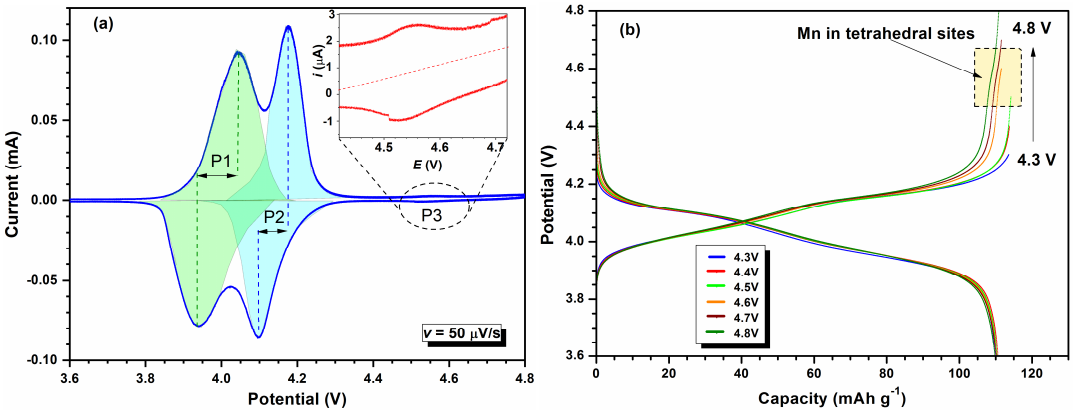

Fig. 1. (a) Cyclic voltammetry profile of 1.5 M $LiPF_6$ EC/EMC (3/7 in w/w) on LMO//Li half-cells performed between 3.6 and 4.8 V (the inset is the magnification of the P3 area). (b) Galvanostatic profiles of the same electrolyte cycled at C/10 under multiple cut-off voltages at room temperature.

A third minor reversible P3 peak in Fig. 1(a), which is highlighted in the plateau Fig. 1(b), is visible around 4.6 V. This is a signature of the presence of manganese in the tetrahedral sites of the material. The presence of this plateau is reported by some authors as an artifact [27]. The cut-off potentials up to 4.8 V vs. Li^+/Li do not seem to have any influence on the galvanostatic profile of the plateaus in both delithiation and lithiation. The redox peaks associated to the two step delithiation are accessible at (4.04 V and 4.17 V), as well at 4.09 V and 3.94 V for lithiation). However, during cycling at high potentials without effective protection, the electrode-electrolyte interfaces degradation generates a rapid loss of capacity.

Discharge capacities obtained in half-cells at 25 °C with 5% (weight) FEC and 1% or 5% TTFP added electrolytes are shown in Fig. 2 and compared to the baseline electrolyte. Initial discharge capacities of the half-cells with FEC added are slightly higher when compared to the standard electrolyte. This gap is maintained during the following cycles and increases when the discharges rates become faster (D-rate as D/2). It is also undeniable that the

presence of FEC stabilizes the capacity, indeed, we observe 23% loss after 20 cycles without FEC versus 16% with FEC. This is mainly due to the effect of the FEC on the lithium electrode, which is known to help form a stable Solid-Electrolyte Interphase (SEI), and supported by the fact that almost no Cathode Electrolyte Interphase (CEI) is formed by FEC on the $LiMn_2O_4$ electrode [19].

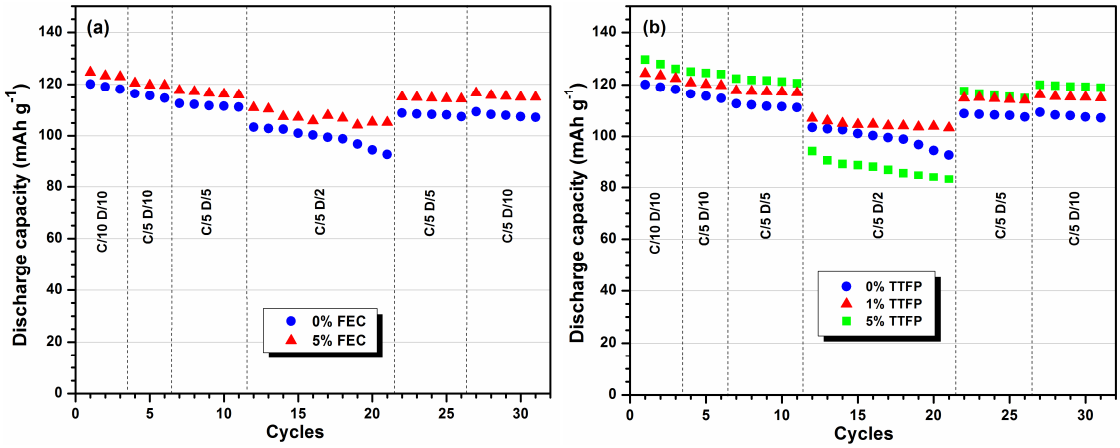

Fig. 2. (a) Discharge capacity of LMO//Li half-cells cycled between 3.2 and 4.7 V at room temperature with 1.5 M $LiPF_6$ in EC/EMC (3/7, w/w), exhibiting the impact of FEC as additive. (b) Different concentrations of TTFP as additive.

Higher discharge capacities are obtained with the TTFP additive (1% and 5%). However, at D/2 the electrolyte containing 5% TTFP is unfavored, due to a reduction of the ionic mobility caused by a low dissociation effect of TTFP. As shown in our previously work, 5% of TTFP additive decreases by 10% the conductivity of EC/DMC 1 M $LiPF_6$ [28]. TTFP and FEC have separate positive impacts, they both act to stabilize their dedicated interface (FEC on Li/electrolyte and TTFP on LMO/electrolyte), and do not disturb the opposite interface. We then seek to see their synergy. Electrolytes containing different mixtures of FEC and TTFP were investigated on half-cells at room temperature and maintaining a maximum concentration of additives at 5% (2.5% + 2.5%) and (4% + 1%) of FEC and TTFP, respectively. Selected galvanostatic profiles and compiled discharge data are displayed in Fig. 3, and compared to the baseline electrolyte (0% additive).

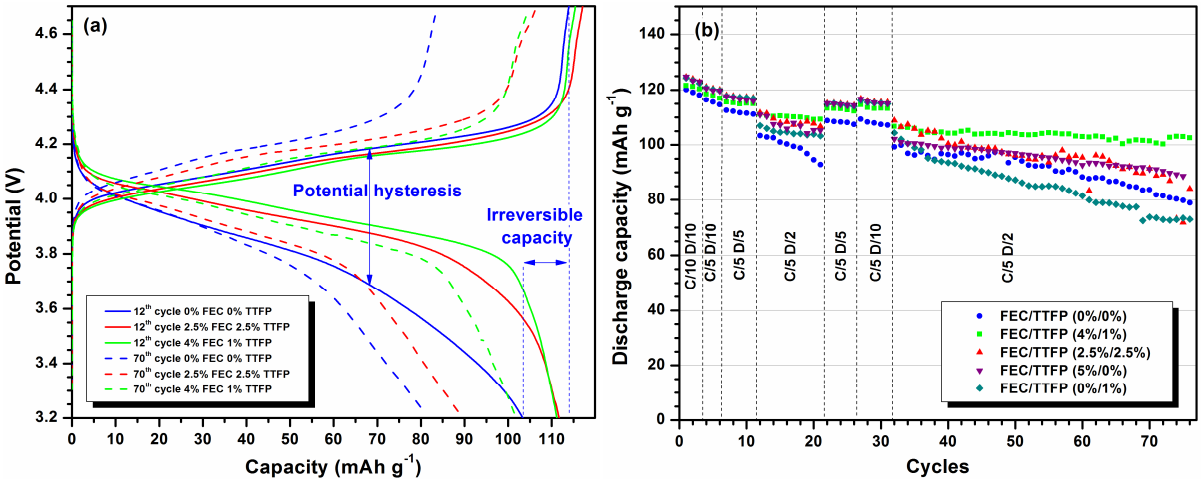

Fig. 3. (a) Galvanostatic profiles of the 12th and the 70th cycle (C/5 D/2) of LMO//Li half-cells cycled between 3.2 and 4.7 V at room temperature with 1.5 M $LiPF_6$ in EC/EMC (3/7, w/w), and two ratios of FEC-TTFP additive combination. (b) Discharge capacities vs. cycle number of the additive containing electrolytes.

In order to clearly observe the evolution of the cycling state of the half-cell systems, as illustrated in Fig. 3(a), the comparative galvanostatic profiles of the 12th and 70th cycles. We can see unambiguously that the potential hysteresis and the irreversible capacity (see Fig. 3a) are much more contained with 4% FEC and 1% TTFP as additives. In the latter case, the decrease on capacity was only 9 mAh g^{-1} between the 12th and 70th cycle, while it was 21 mAh g^{-1} and 23 mAh g^{-1} for the electrolyte containing the same concentration of FEC and TTFP and the baseline electrolyte respectively. The potential hysteresis reflects increasing resistance in the system, possibly due to thick film formation on the lithium metal anode and LMO cathode in the absence (or the inadequate proportion) of additives.

Looking at the Fig. 3(b), the same initial capacities were obtained with both electrolytes containing two additives, independently to their proportions, and were better than standard additive-free electrolyte. During each charge/discharge cycle, at different C-rates, the evolution of the capacities vs. cycle number was closer to the baseline electrolyte, namely fading rapidly from 109 mAh g^{-1} to 84 mAh g^{-1} (an average of 0.61 mAh g^{-1} per cycle). Unless for the (C/5-D/2) 10 cycles, where performances in presence of additives appeared clearly more stable than the reference.

Regarding the long-term cyclability, better capacity retention was obtained with the combination of 4% FEC and 1% TTFP. Over this period, capacities were only fading from 106 mAh g^{-1} to 102 mAh g^{-1} (an average of 0.1 mAh g^{-1} per cycle). The electrolyte with 4% FEC and 1% TTFP added showed an interesting ability to reduce the fading of a $LiMn_2O_4$ electrode, considering that the $LiMn_2O_4$ electrode is sensitive at high potentials to oxygen loss and subject, as all metal oxide type cathodes, to radical oxygen species attack ($O_2^{\cdot -}$; $O^{\cdot -}$, O^{2-}). When the $LiMn_2O_4$ electrode reaches a high potential (> 4.5 V), extrusion of oxygen species ([O]) can occur, and react with the SEI and weaken it [8,29]. The resulting Mn^{3+} ions undergo a disproportionation reaction on the surface of the LMO cathode particles, and Mn^{2+} ions, which readily dissolve into the electrolyte and further increase the fading of the cells: ($2Mn^{3+}_{(cathode)} \rightarrow Mn^{4+}_{(cathode)} + Mn^{2+}_{(electrolyte)}$)

It is now well known that TTFP is an efficient "oxygen scavenger" and can easily trap oxygenated species to produce stable and soluble phosphates [30,31].

3.1.2. Full-cell systems and consequences on the graphite anode

The formation of SEI on the graphite anode has a decisive role in the de-solvation of lithium ions and is more sensitive to the composition of the electrolyte and its additives. Thus, the quantities and the nature of the additives can change the thickness, the composition and as a consequence on SEI quality. The presence of FEC-oligomers and lithium phosphate salts derived from decomposition of FEC and TTFP in organic, inorganic and polymeric phases of SEI has a significant influence on the performance of the graphite anode [19].

Electrolytes based on EC/EMC with additives mixture (FEC + TTFP) were further investigated in Gr//LMO full-cells, discharge capacities and coulombic efficiencies obtained during galvanostatic cycling at room temperature are plotted in Fig. 4. The electrolyte containing 2.5% FEC and 2.5% TTFP appeared to be the least efficient, with capacities for

each rate being the lowest, especially at 1 C. This additive composition seems to perform but not well enough. Surprisingly, capacities from the best electrolyte in half-cell (4% FEC 1% TTFP) were inferior to that of the baseline electrolyte during cycling at C/10 and C/5, and also when the rate was returning to C/5 between the 29th and the 34th cycle.

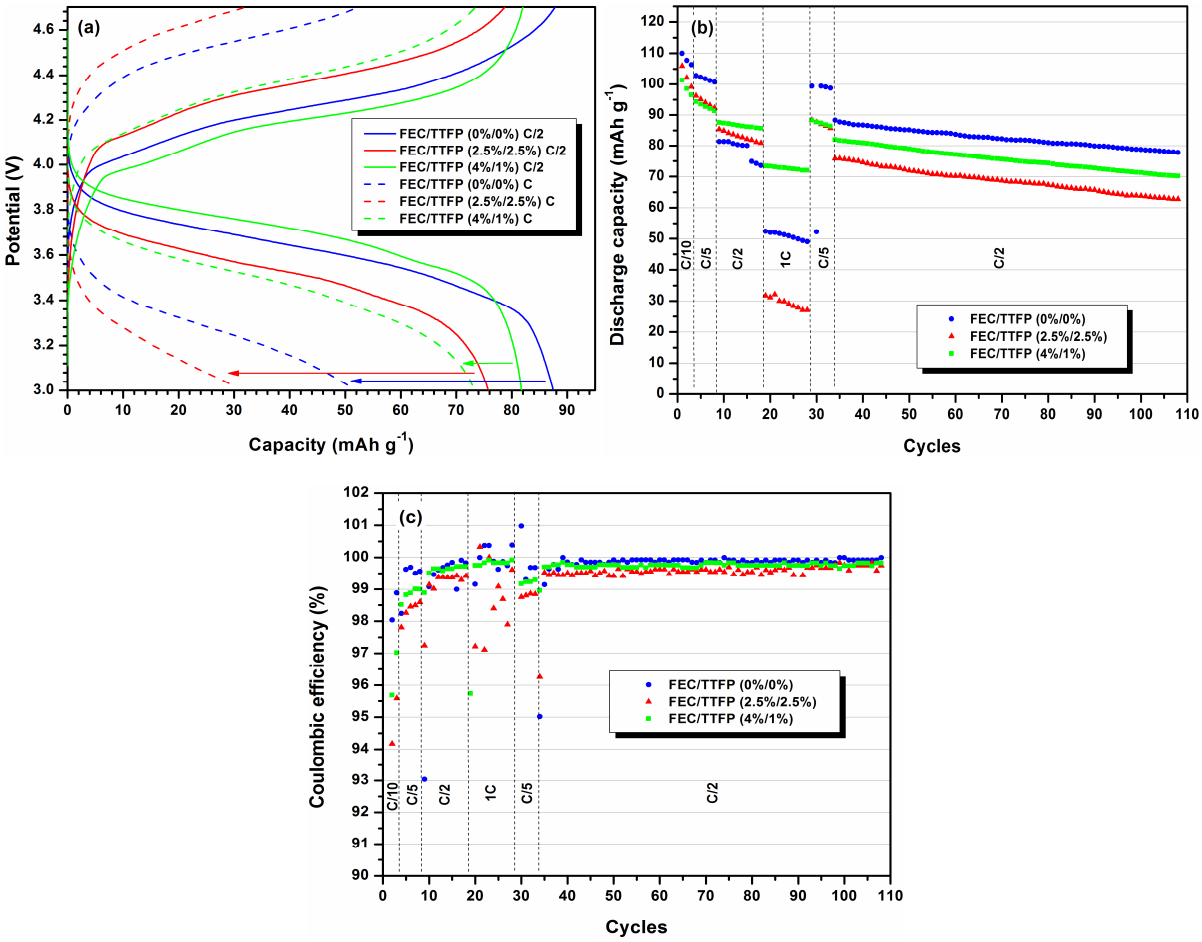

Fig. 4. (a) Galvanostatic profiles at C/2 and C of Gr//LMO cells cycled between 3.0 and 4.7 V at room temperature with 1.5 M $LiPF_6$ in EC/EMC (3/7, w/w), and two combination of FEC-TTFP as additive. (b) Corresponding discharge capacities. (c) Corresponding coulombic efficiencies.

During faster cycling rates (C/2 and 1 C), capacities of the additive-free electrolyte are lower and the positive impact of FEC-TTFP combination of additives is established. During the 75 cycles of second phase at C/2 rate, discharge capacities of FEC and TTFP added electrolyte are inferior to those of the baseline electrolyte. During this phase, the fading of each electrolyte is similar, 0.142 mAh g^{-1} and 0.152 mAh g^{-1} for the baseline electrolyte and the electrolyte with 4% FEC and 1% TTFP respectively. The coulombic efficiency is more stable

for the mixture of 4% FEC and 1% TTFP, particularly when rates of charge and discharge are fast (C/2 and 1C). During the long-time cycling, at C/2, the coulombic efficiencies reach an average of 99.9% for the baseline electrolyte, versus 99.7% for the best additive electrolyte.

The obtained results show that with enough FEC, the performances at high rates are improved thanks to a good quality of SEI on the negative electrode. It as has been demonstrated by Lu *et al*., that the SEI on the graphite formed by the reduction of the FEC is less resistive than those formed by the usual alkyl carbonates, and allows for faster intercalation/deintercalation [19,32]. On the other side, the FEC does not protect the surface of $LiMn_2O_4$ electrode. At the same time the presence of TTFP cannot be neglected with respect to the SEI and can interfere with carbonates on SEI formation, modifying the system performances [23,34]. To summarize, as illustrated in Scheme 1, against surface phenomena of LMO, the combination in adequate proportions of fluorinated additives can be the solution to avoid not only the attack on the LMO-cathode (TTFP role) but also to prevent the consequences on the Li-metal or graphite-anode (FEC role) [19,35]. However, it is important to refine the optimal amounts of the two additives according to the intended application: high power or high energy density.

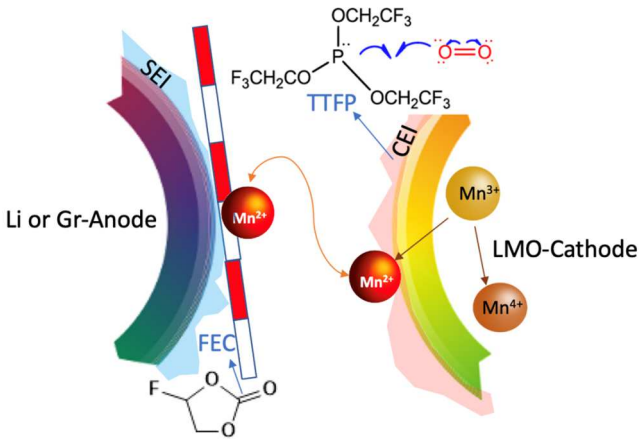

Scheme 1. Schematic presentation for the protective action of delithiated LMO cathode by TTFP and Li or Gr anode by FEC toward manganese dissolution and attack.

3.2. Effect of fluorinated solvent on LMO performances

Generally, the introduction of fluorine on a solvent molecule results in the drop of energy levels for both the highest occupied molecular orbital (HOMO) and the lowest unoccupied molecular orbital (LUMO), leading generally to higher resistance against oxidation [36]. It could also signify better (denser) SEI film as the formation starts at a higher potential. For this reason, there have been numerous efforts in fluorinating both cyclic and acyclic carbonates. Before carrying out the electrochemical characterizations of cell by modifying the electrolyte, the influence of TFEMC as co-solvent on transport properties of electrolytes was studied. To understand the role of the fluorinated solvent on the behavior of graphite and LMO interfaces, we chose an EMC homolog, the 2,2,2-trifluoroethyl methyl carbonate (TFEMC) due to its high potential stability demonstrated on $LiNi_{0.5}Mn_{1.5}O_4$, and also as it appears to react on the surface of NMC_{532} electrode and form a CEI on this type of electrode [26,37]. To the best of our knowledge, no publications or information could be found on the use of TFEMC as an additive or co-solvent on Gr//LMO full-cell.

3.2.1. Transport properties of electrolytes containing TFEMC

The major difference between EMC and TFEMC lies in the charge distribution induced by the fluorine atoms, this modifies the HOMO LUMO orbitals of the molecule. As shown in Table 1, the values are obtained by Gamess Ab-initio calculations, basis set: routine 6-31G(d) calculation of molecular orbital on RHF theory with singlet multiplicity. It can be seen in Table 2 that on the TFEMC there are two zones of negative charge density: one on carbonate oxygen atoms, and the second on the fluorine atoms. This induces on the one hand a different solvation model of Li^+ cation in comparison with EMC, and on the other hand, higher intermolecular interactions between two TFEMC solvent molecules, these inter-molecular interactions are inexistent between two EMC molecules.

Table 1. Comparatives characteristic values obtained by Gamess Ab initio calculations (basis set: routine 6-31G(d) calculation of molecular orbital on RHF theory with singlet multiplicity).

Molecule	EMC	TFEMC
Structure	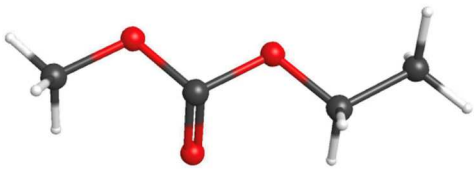	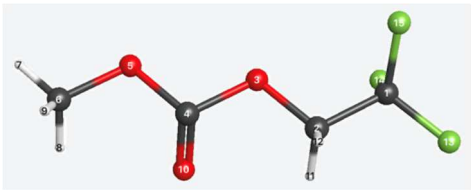
Charge[a]	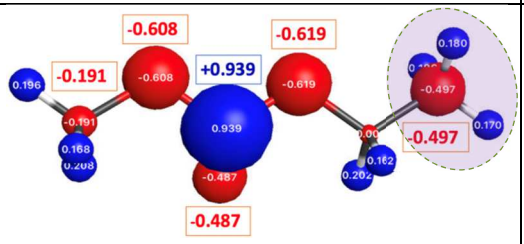	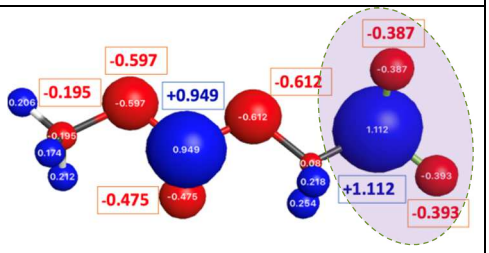
Li^+ solvation model	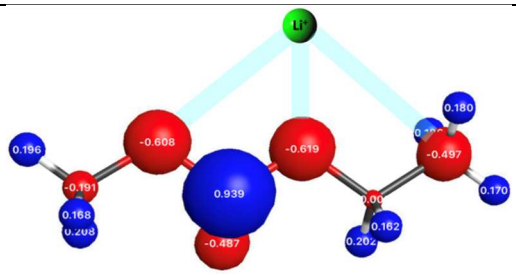	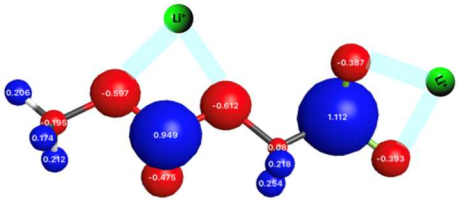
HOMO (Hartree)[b]	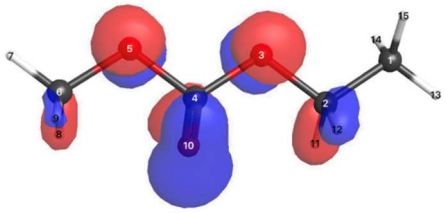 -0.4420	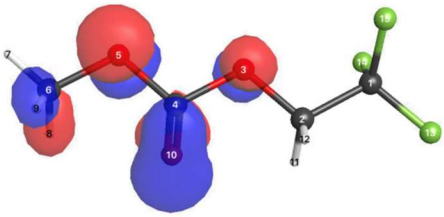 -0.4682
LUMO (Hartree) [b]	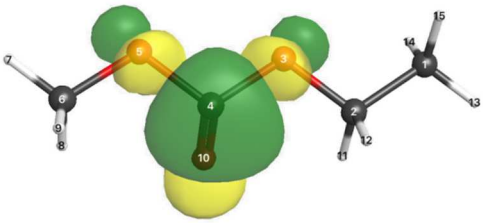 0.0471	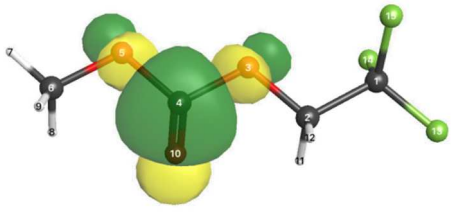 0.0211

[a] The size of the spheres is relative to the charge density (blue = positive, red = negative);
[b] 1 Hartree = 27.2114 eV

We also notice that the energy levels of the HOMO and LUMO frontier orbitals are such that the TFEMC resists better on both reduction (lower HOMO energy) and oxidation (lower LUMO energy), as shown in Scheme 2.

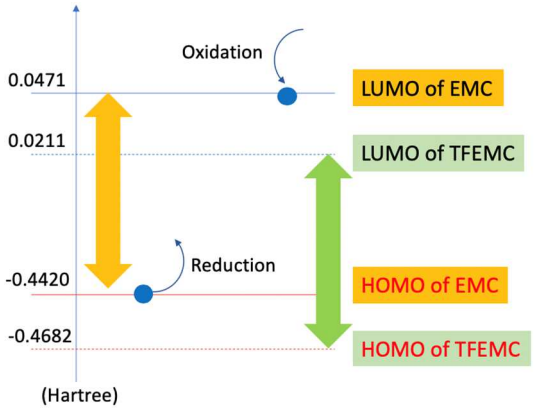

Scheme 2. HOMO and LUMO limits orbital for EMC and TFEMC and their effect on expected electrochemical stability.

The three electrolytes were formulated by keeping the proportion of EC constant and by varying the proportion of EMC (1-x)%/x% TFEMC ratio such that (EC/(1-*x*)EMC/ *x*TFEMC ratio (*x* = 0, 10%, 30% and 50%) by weight. Ionic conductivities and viscosities with and without 1.5 M $LiPF_6$ were measured over an extended temperature range and plotted together in Fig. 5 as well as their VFT fitting. The conductivities decrease with higher TFEMC percentage: $\sigma_{0\%TFEMC} > \sigma_{10\%TFEMC} > \sigma_{30\%TFEMC} > \sigma_{50\%TFEMC}$ (Fig. 5a). Moreover, the difference between $\sigma_{0\%TFEMC}$ and $\sigma_{X\%TFEMC}$ diverges when the temperature is increased to 353 K, from 0.85 mS cm^{-1} to 1.62 mS cm^{-1}, respectively.

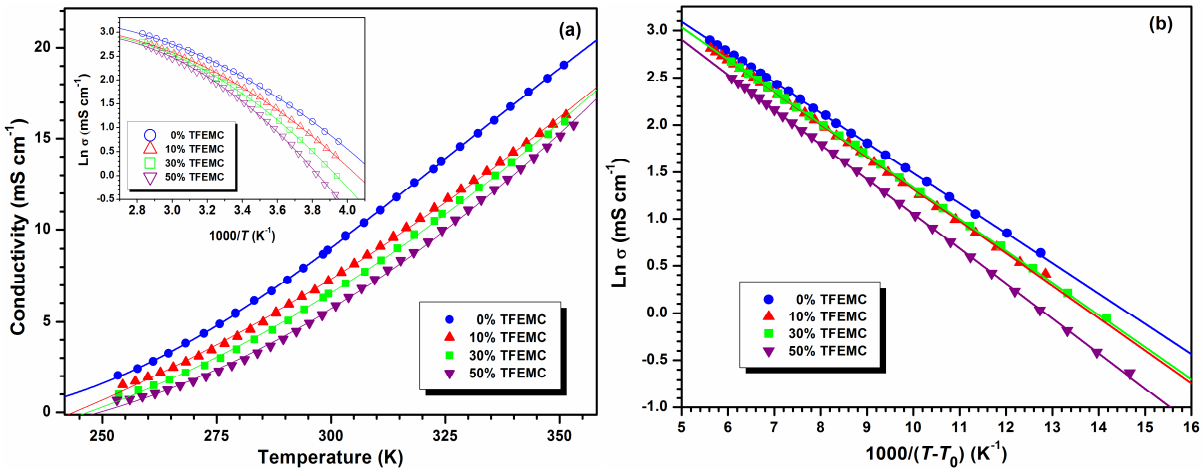

Fig. 5. (a) Ionic conductivities of 1.5 M $LiPF_6$ in EC/EMC/TFEMC (3/7–*x*/*x*) with *x*=0,1,3,5 (the inset is the Arrhenius plot). (b) Corresponding VFT fitting.

Ion mobility in solution is the result of several parameters which result from both solvent and salt interactions. Ions are subjected, in solution, to both ionic associations (cation/anion) and to influence the solvation from alkyl carbonates (fluorinated and non-fluorinated). They undergo the effect of the temperature which disturbs the equilibrium, acting on both ion-pairing and on the solvation sphere, and sometimes in an antagonist way. It is difficult to deconvolute the interactions in solutions; however, the viscosity is linked to the Wan der Waals forces (solvent/solvent), as a consequence the introduction of TFEMC is more sensitive to temperature changes.

Fig. 6(a and b) illustrates the influence of TFEMC addition on viscosity of the ternary solvent mixture. The increase in viscosity is significant when replacing 10% of EMC by the TFEMC. At 25 °C the viscosity increases by 30% going from 1 to 1.3 mPa s, this increase is attenuated beyond 30% of TFEMC in electrolyte. In the presence of 1.5 M $LiPF_6$ salt, the viscosity is 8 times greater than for 0%, and for 10% TFEMC by comparison is almost 10 times higher with 1.5 M of salts at low temperature (T = 10 °C) and with 50% of TFEMC. It is remarkable to notice that the effect of temperature is more pronounced in the presence of $LiPF_6$, which indicates that ionic associations and solvation are the two major phenomena affected by temperature, much more than solvent-solvent interactions.

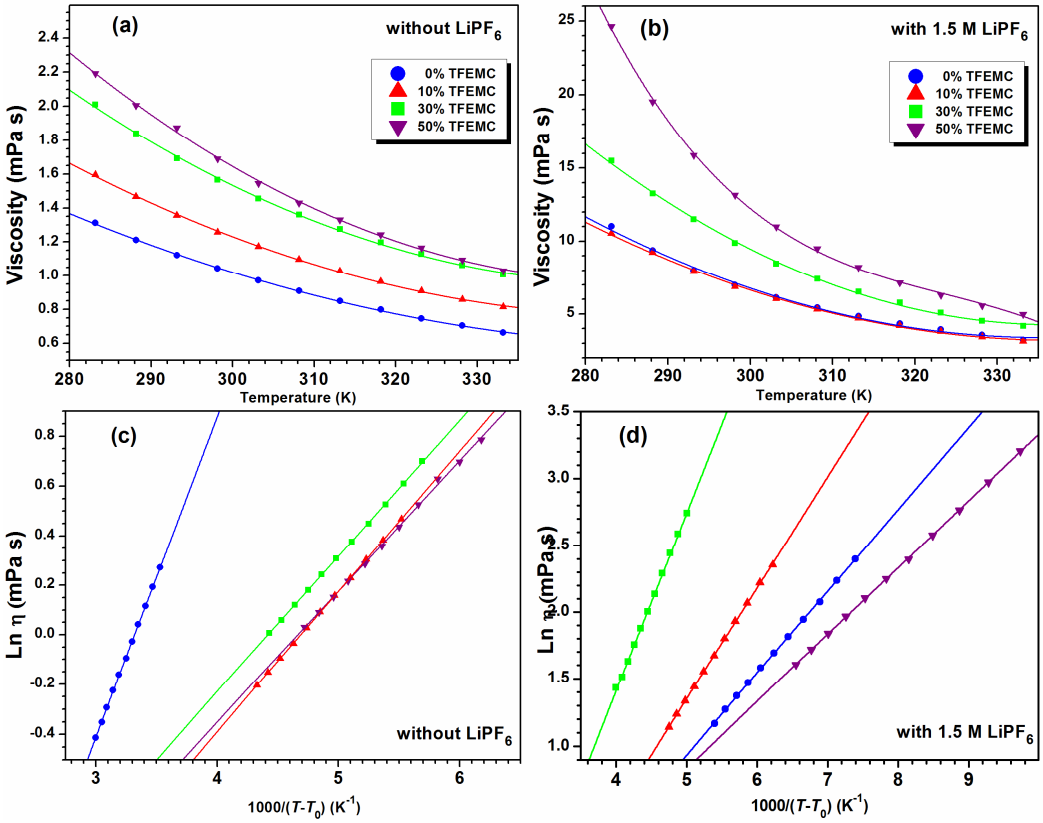

Fig. 6. (a) Viscosities of EC/EMC/TFEMC (3/7-*x*/*x*) with *x*=0,1,3,5 without $LiPF_6$. (b) With 1.5 M $LiPF_6$. (c, d) Corresponding VFT fitting.

Both conductivity and viscosities values of electrolyte solutions have a non-Arrhenius ($\ln(\sigma) = f\left(\frac{1}{T}\right)$) behavior between 283 K and 353 K, (inset in Fig. 5a for conductivities) but are correctly modeled by the Vogel-Fulcher-Tamman (VFT) equations (Eqs. (1) and (2)).

$$\sigma = \sigma_0 \exp\left(\frac{-B_\sigma}{R}\left[\frac{1}{T-T_0}\right]\right) \quad (1)$$

$$\eta = \eta_0 \exp\left(\frac{-B_\eta}{R}\left[\frac{1}{T-T_0}\right]\right) \quad (2)$$

Fitting parameters T_0, B_σ , B_η σ_0 , and η_0 are summarized in Table 2.

Table 2. VFT fitting parameters of conductivities and viscosities with and without 1.5 M $LiPF_6$ for the four investigated mixtures.

Sample	Conductivity	Viscosity

	1.5 M $LiPF_6$			0.0 M $LiPF_6$			1.5 M $LiPF_6$		
	$B_\sigma \times R$	T_0	R^2	$B_\eta \times R$	T_0	R^2	$B_\eta \times R$	T_0	R^2
0% TFEMC	2.67	175.01	0.9999	10.70*	/	0.9999	5.08	147.92	0.9998
10% TFEMC	2.82	176.67	0.9998	4.68	102.09	0.9999	6.90	122.49	0.9998
30% TFEMC	2.77	185.01	0.9998	4.55	107.52	0.9999	11.08	83.36	0.9996
50% TFEMC	3.01	187.56	0.9999	4.37	121.44	0.9989	4.15	180.43	0.9999

*Fitted with Arrhenius model.

The ideal glass transition temperature T_0, obtained with ionic conductivities or viscosities without salt are homogeneous with less than 10 K of deviation. With 1.5 M $LiPF_6$, the viscosities show more fluctuation in T_0 according the composition of electrolyte. A 30% TFEMC composition possess the smallest T_0 value (T_0 = 83.36 K) and the largest pseudo activation energy ($B_\eta \times R = 11$ kJ mol^{-1}). Moreover, this value is doubled for the viscosity without salt when compared to the conductivity with salt, which signifies that solvent-solvent interactions are weakened with the introduction of the $LiPF_6$ salt. This is likely due to more favorable solvent-ion interaction allowing for ionic mobility, which sees a decrease in the activation energy. It means that the introduction of TFEMC mostly affects viscosity particularly when a salt is present.

The Walden plot ($W = \Lambda \times \eta$) represents the reciprocal dependence of viscosity and molar conductivity for an ionic solution against temperature [38]. The correlation between conductivity and fluidity should keep the Walden product, *W,* constant with temperature if no factor other than viscosity of the solution hinders the diffusion of ions [39-41]. A negative slope suggests that there is no modification in the solvation of ions over the temperature range studied [38,42]. In the opposite case, with a positive slope, the inherent viscosity is superior implying a modification in ions solvation and finally more solvent molecules engaged into the

solvation process. For the four electrolytes studied here, (see Fig. 7a) the *W* evolution appears to be strongly dependent on temperature and composition for each case and diminish with decreasing temperature.

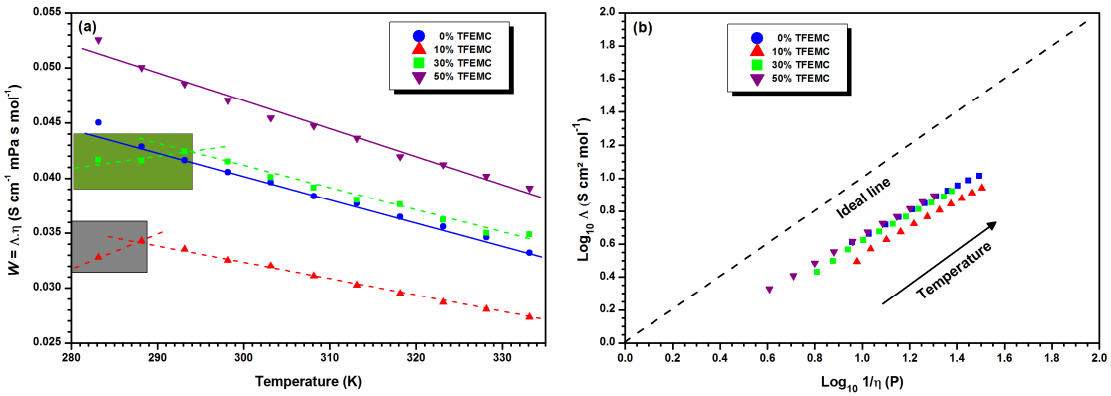

Fig. 7. (a) Walden product vs. temperature of 1.5 M $LiPF_6$ in EC/EMC/TFEMC (3/7-*x*/*x*) with *x*=0,1,3,5. (b) Corresponding Walden Plot.

For the two-extreme compositions, (0% and 50% of TFEMC) *W* values are following an almost constant decrease over the temperature range, this is due to the faster diminution of the viscosity than the increases of the ionic conductivity. This means that when the temperature increases, the viscosity decreases faster than the conductivity and does not compensate it. Indeed, the mobility of the ions is a process which requires less energy than the viscous flow as we saw previously. For the two intermediate compositions (10% and 30%), we observe two different zones of *W* evolution, before 288 K, where ionic dissociation favors the conductivity without being hindered by solvation, *W* increases beyond this temperature as the behavior becomes standard. For the rest of the compositions the solvent interactions predominate and decrease the viscosity more quickly.

In absence of TFEMC, a solvation model is based on strong EMC-Li interaction thanks to charge distribution as shown in Table 1 using molecular calculation. While TFEMC can complex two Li^+ cations differently and present intermolecular interactions, due to the presence of fluorine atoms, these two different organizational models in solution are predominant at two-extreme compositions (0% and 50% of TFEMC) respectively and are

affected similarly by temperature. The intermediates concentrations (10% and 30% of TFEMC) represent a mix of the two models which can explain the variations in behavior observed with regard to the temperature, as well as the slope break when switching from one model to another under the effect of temperature.

Fig. 7(b) shows the Walden plot representing the ionicity evolution vs. temperature of the four electrolytes. The observed curves are almost identical and show parallel slopes to the KCl ideal curve. This means that on the one hand the ionic dissociation is similar for all the electrolytes studied and that the differences in viscosity are essentially due to the interactions between the solvent (TFEMC) and not the ionic associations. Knowing that in Li-ion batteries, a key factor is the transport number of the Li^+ cation, and consequently the ionicity, we can therefore predict that there will be no strong negative impact from the introduction of TFEMC on the battery performance [43,44].

3.2.2. Incidence of TFEMC as co-solvent on galvanostatic performances on Gr//LMO

Our four electrolytes containing 1.5 M $LiPF_6$ with ternary mixture (EC/EMC/TFEMC; 3/7-*x*/*x*) where x = (0,1,3,5) were evaluated by galvanostatic cycling, in Gr//LMO full-cell at different C-rate. Selected comparative galvanostatic profiles, of the 36th cycle, are presented in Fig. 8. The effect of the addition of TFEMC is visible on the resistance of the cell and therefore the differences in the plateaus-potentials of the charge-discharge. The 30% TFEMC composition is optimal, while 10% and 50% show respectively, an increase in cell resistance (+ 60%; ΔE = 0.8 V and 0.5 V, Fig. 8) and a decrease in capacity (-17%) when compared to the optimal composition of 30%.

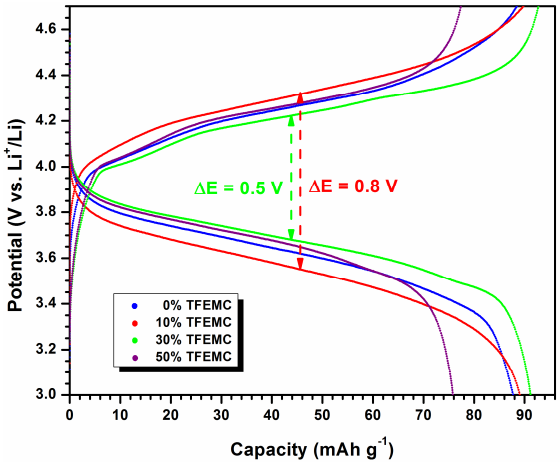

Fig. 8. Galvanostatic profile at C/2, of Gr//LMO cell cycled between 3.0 and 4.7 V at room temperature with $LiPF_6$ 1.5 M in EC/EMC/TFEMC (3/7-*x*/*x*) with *x* = 0,1,3,5.

Fig. 9(a and b) represents, for the Gr//LMO system, the obtained discharge capacities and coulombic efficiencies, respectively. The coulombic efficiencies exceed 99% and are stable for all composition during all rates, with an average of 99.81% over 75 cycles at C/2 for 30%, compared to 99.80%, 99.60% and 99.76%, for the baseline electrolyte, 10% TFEMC and 50% TFEMC respectively. The electrolyte containing the lowest concentration of TFEMC (10%), the capacities were globally elevated except for the highest rate (1C, 45 mAh g^{-1}), where this electrolyte seems to be penalized by the reduced concentration of fluorinated molecules, and tend towards the baseline electrolyte behavior, the non-fluorinated. With 30% TFEMC, the optimum stability and highest capacities at C/2 and 1 C are obtained. Finally, with a 50% of TFEMC, passivation of the cathode and de-solvatation of Li^+ does not compensate the negative impact of the viscosity and induce stable cycling, but with much lower capacities. These results show that there is competition between protective aspect of TFEMC and its viscosity (η = 1) than the EMC (η = 0.65), [45] during high C-rate, and therefore a brake during high rate cycling in favor of 30% TFEMC. Concerning coulombic efficiencies, they are more stable than the baseline electrolyte and the one containing 10% TFEMC, however, they were generally lower than those of the electrolyte containing 30% of TFEMC and those of the reference electrolyte. The capacities associated to the electrolyte containing 30% of

TFEMC were very close to the highest at a low rate (105 mAh g^{-1} at C/10 and 100 mAh g^{-1} at C/5). In addition, those obtained at high rates (C/2 and 1 C) were the highest (95 and 80 mAh g^{-1}). Since neither the conductivity or the ionicity show an obvious superiority of the transport properties of TFEMC, when compared to the standard electrolyte, it is logical to think that TFEMC essentially acts at the interface. By less complexing the Li^+ cation, it facilitates its de-solvation and by consequence its intercalation.

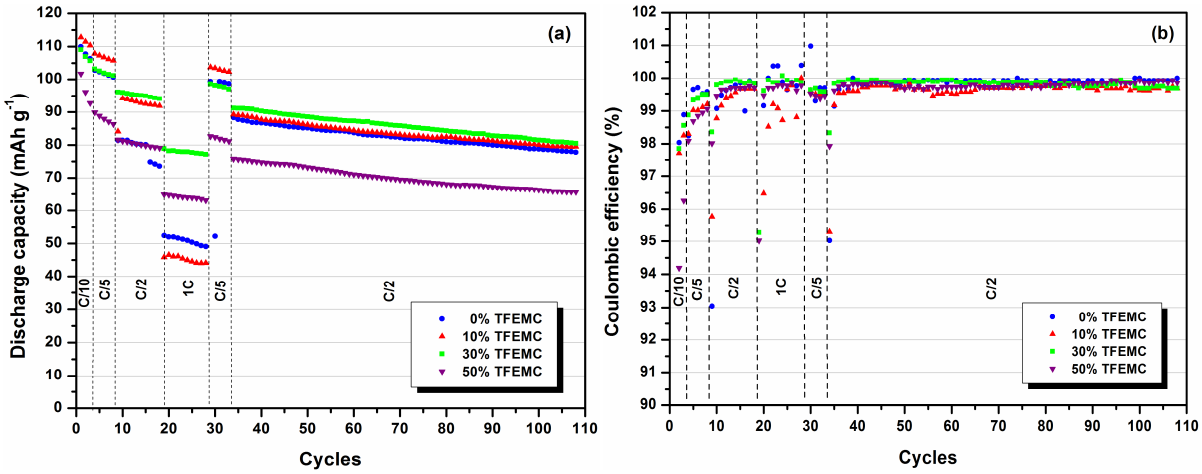

Fig. 9. (a) Discharge capacities of Gr//LMO cells cycled between 3.0 and 4.7 V at room temperature with $LiPF_6$ 1.5 M in EC/EMC/TFEMC (3/7-*x*/*x*) with *x* = 0,1,3,5. (b) Corresponding coulombic efficiencies.

3.2.3. Electrochemical impedance spectroscopy, TFEMC action

In order to investigate the action of the TFEMC on LMO cathode, impedance measurements were performed in half-cells on the most efficient electrolyte, i.e. 30% of TFEMC. High-to-medium frequency contribution of obtained data at discharged state of 3.2 V between 1 mHz to 1 MHz are displayed as a Nyquist plot in Fig. 10. We assume that the redox reaction on the lithium anode is significantly faster compared to the electron transfer and Li intercalation on $LiMn_2O_4$ electrode in freshly prepared cells. The contribution of the negative electrode can be neglected, [46] and impedances curves presented in the Fig. 10 show the interfacial impedance on the $LiMn_2O_4$ electrode.

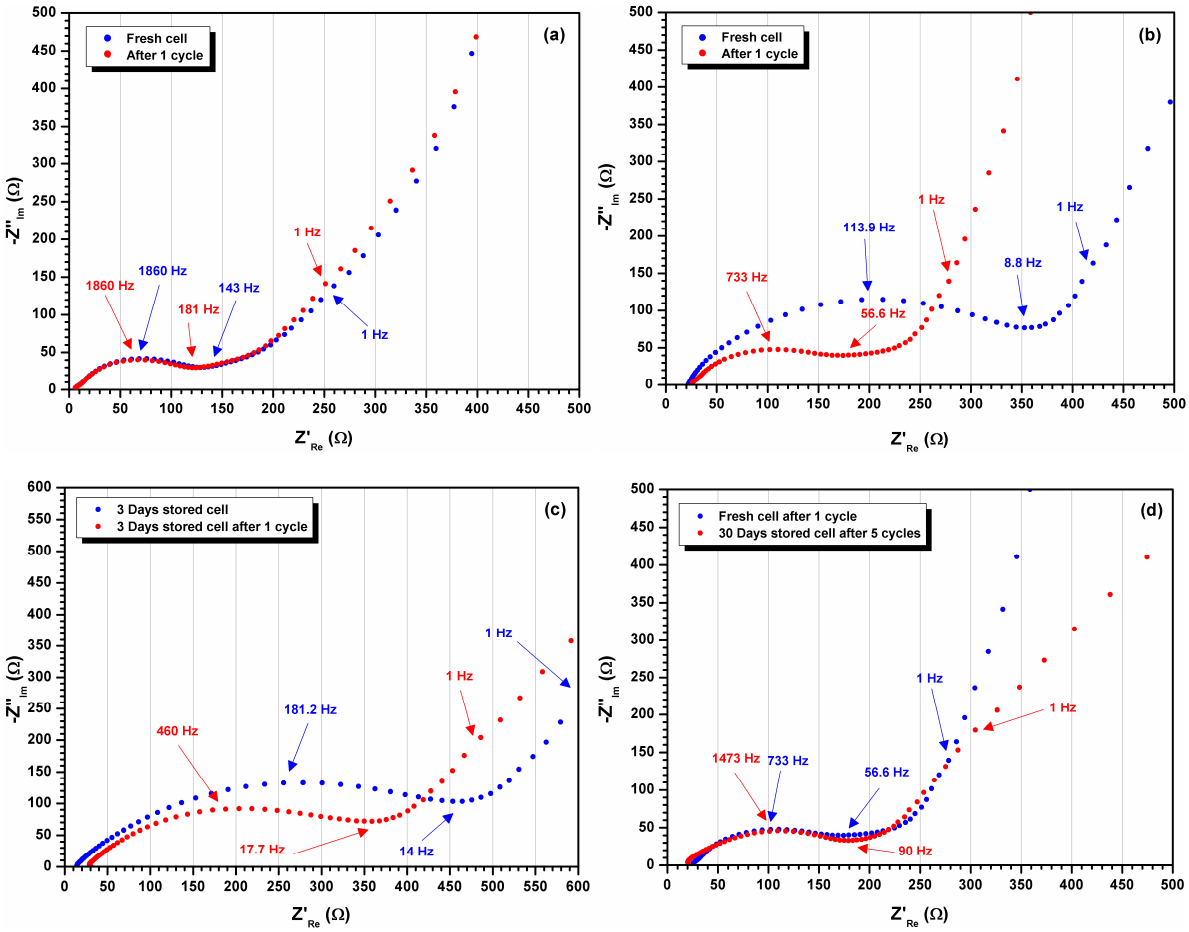

Fig. 10. (a) EIS profiles at 3.2 V of LMO//Li half-cells filled with $LiPF_6$ 1.5 M in EC/EMC (3/7). (b,c,d) EIS profiles at 3.2 V of freshly prepared or stored (25 °C) of LMO//Li half-cells filled with 1.5 M $LiPF_6$ in EC/EMC/TFEMC (3/4/3).

Firstly, the impedances from the reference electrolyte are plotted in Fig. 10(a), the differences between the curves obtained with a non-cycled cell and after its first cycle are very small. The two visible semicircles almost overlap, and reach both a resistance around 110 Ω. The alkyl carbonates (EC, EMC) are known to passivate very weakly positive electrodes, especially on fresh cells, [47] we can therefore consider the semicircles of Fig. 10(a) as only the charge-transfer resistance and global curves as the representation of the absence of CEI on $LiMn_2O_4$. The same impedance measurement protocol was applied to the electrolyte containing 30% TFEMC (Fig. 10b), the curve obtained with a non-cycled cell was very different from that obtained previously. The diameter of the first semicircle reaches of 325 Ω and deconvoluted in two semicircles because of its flatness, which will indicate the presence of a passivation layer from the TFEMC.

It is interesting to notice that it was formed at open circuit voltage, and so that it is intrinsically related to the reactivity of TFEMC toward the positive electrode. After a single galvanostatic cycle, the diameter of the semicircle was greatly reduced (150 Ω) with also a very flat shaped semicircle. If we consider the coexistence of two semicircles and subtract the 110 Ω of the charge transfer resistance, there remains a resistance of 40 Ω attributable to the formation of a CEI. In Fig. 10(c), are the plotted impedance measurements of a three-day stored cell before and after one cycle. A wide semicircle compared to the one obtained previously with the same electrolyte is present and has a larger diameter of 438 Ω. It is therefore reasonable to think that this pre-cycling resistance is related with the storage time. After cycling, there is a reduction in resistance of this semicircle, which is established at 332 Ω (-106 Ω). This decrease in one cycle is less important than the previous (-175 Ω) and can come from a larger deposit on the electrode caused by a longer exposure of the electrolyte to the positive electrode at the open-circuit voltage. Moreover, the solution resistance is almost multiplied by two after one cycle which could be imputed to the solubilisation of a part of the CEI into the electrolyte modifying the transport properties of the latter. Finally, we wanted to demonstrate the resilience of the passivation layer with respect to the storage time, the obtained results are illustrated in Fig. 10(d). A cell which was stored for 30 days showed impedance very close to a one-time cycled non-stored cell, in five galvanostatic cycles. Only the diffusion region seems to be affected, with an inferior slope related to a slower diffusion in the bulk. This difference is probably produced by the long storage period of the cell. The diameter of the semicircle was 159 Ω, whereas it was 150 Ω for the fresh cell. By using previous hypothesis (subtraction of 110 Ω) the residual charge transfer resistance should be 49 Ω for the CEI, which constitutes a weak increase (+ 9 Ω) and demonstrates that the increasing impedance observed during the open-circuit voltage is almost completely reversible while keeping a passivation layer on the surface of the positive electrode. This is

proof that the protection of TFEMC is essentially due to its action at the interface like fluorinated additives, even if this action is different in nature. On the one hand the easy de-solvation of lithium cation and on the other hand participation in the CEI quality.

4. Conclusions

In summary, a combination of fluorinated additives, FEC and TTFP, was optimized and cycled on LMO//Li half-cells at a high potential (4.7 V). The transition into full-cells with a graphite anode revealed that the combination in adequate proportions of fluorinated additives can be the solution to avoid not only the attack on the LMO-cathode (TTFP role) but also to prevent the consequences on the Li-metal or graphite-anode (FEC role). However, it is important to refine the optimal amounts of the two additives according to the intended application, high power or energy density. The second part of this study focused on the effect of fluorinated TFEMC as co-solvent. By optimizing the proportion of TFEMC in the electrolyte, we showed that in a full-cell, good electrochemical performance during fast galvanostatic cycling and satisfactory capacity retention during long-term cycling were obtained. Finally, the EIS investigation of the LMO/electrolyte interface containing TFEMC demonstrates that despite a high reactivity of the electrolyte towards the positive electrode, characterized by a significant and increasing resistance over time, which is reversible in few cycles and could generate a passivation layer on the surface that is not too resistive and good quality. We show in this study that the approach based on the TFEMC and Li^+ ions solvation has as much impact on Gr//LMO full-cell performance than CEI and SEI dedicated additives (FEC and TTFP). In conclusion, whether in the form of additives or co-solvents, the fluorinated compounds studied here are beneficial to the cyclability of the Gr//LMO system and act essentially at the interface by controlling the solvation of lithium-ion or the quality of the CEI.

Acknowledgments

The authors would like to thank “La region Centre Val de Loire” for financial support to the researchers involved in this study on OBAMA project under “Lavoisier II” regional program.

References

[1] J.M. Tarascon, M. Armand, Nature 414 (2001) 359-367.
[2] B. Dunn, H. Kamath, J.-M. Tarascon, Science 334 (2011) 928-935.
[3] V. Etacheri, R. Marom, R. Elazari, G. Salitra, D. Aurbach, Energy Environ. Sci. 4 (2011) 3243-3262.
[4] N.-S. Choi, Z. Chen, S.A. Freunberger, X. Ji, Y.-K. Sun, K. Amine, G. Yushin, L.F. Nazar, J. Cho, P.G. Bruce, Angew. Chem. Int. Ed. 51 (2012) 9994-10024.
[5] M. Armand, J.M. Tarascon, Nature 451 (2008) 652-657.
[6] Y. Nishi, J. Power Sources 100 (2001) 101-106.
[7] O.K. Park, Y. Cho, S. Lee, H.-C. Yoo, H.-K. Song, J. Cho, Energy Environ. Sci. 4 (2011) 1621-1633.
[8] G. Xu, Z. Liu, C. Zhang, G. Cui, L. Chen, J. Mater. Chem. A 3 (2015) 4092-4123.
[9] J.M. Tarascon, E. Wang, F.K. Shokoohi, W.R. McKinnon, S. Colson, J. Electrochem. Soc. 138 (1991) 2859-2864.
[10] M. Wohlfahrt-Mehrens, C. Vogler, J. Garche, J. Power Sources 127 (2004) 58-64.
[11] B. Koo, J. Lee, Y. Lee, J.K. Kim, N.-S. Choi, Electrochim. Acta 173 (2015) 750-756.
[12] R.J. Gummow, A. de Kock, M.M. Thackeray, Solid State Ionics 69 (1994) 59-67.
[13] M.M. Thackeray, Y. Shao-Horn, A.J. Kahaian, K.D. Kepler, E. Skinner, J.T. Vaughey, S.A. Hackney, Electrochem. Solid-State Lett. 1 (1998) 7-9.
[14] Y. Xia, Y. Zhou, M. Yoshio, J. Electrochem. Soc. 144 (1997) 2593-2600.
[15] Z. Chen, K. Amine, J. Electrochem. Soc. 153 (2006) A316-A320.
[16] B. Li, Y. Wang, H. Rong, Y. Wang, J. Liu, L. Xing, M. Xu, W. Li, J. Mater. Chem. A 1 (2013) 12954-12961.
[17] X. Zuo, J. Wu, C. Fan, K. Lai, J. Liu, J. Nan, Electrochim. Acta 130 (2014) 778-784.
[18] N.-S. Choi, J.-G. Han, S.-Y. Ha, I. Park, C.-K. Back, RSC Adv. 5 (2015) 2732-2748.
[19] H. Shin, J. Park, A.M. Sastry, W. Lu, J. Electrochem. Soc. 162 (2015) A1683-A1692.
[20] W. Li, C. Campion, B.L. Lucht, B. Ravdel, J. DiCarlo, K.M. Abraham, J. Electrochem. Soc. 152 (2005) A1361-A1365.
[21] Y. Liu, L. Tan, L. Li, J. Power Sources 221 (2013) 90-96.
[22] T. Li, X.-Q. Zhang, P. Shi, Q. Zhang, Joule 3 (2019) 2647-2661.
[23] E. Markevich, G. Salitra, D. Aurbach, ACS Energy Lett. 2 (2017) 1337-1345.
[24] X.-Q. Zhang, X. Chen, X.-B. Cheng, B.-Q. Li, X. Shen, C. Yan, J.-Q. Huang, Q. Zhang, Angew. Chem. Int. Ed. 57 (2018) 5301-5305.
[25] X. Fan, L. Chen, O. Borodin, X. Ji, J. Chen, S. Hou, T. Deng, J. Zheng, C. Yang, S.-C. Liou, K. Amine, K. Xu, C.Wang, Nat. Nanotechnol. 13 (2018) 715-722.
[26] J. Im, J. Lee, M.-H. Ryou, Y.M. Lee, K.Y. Cho, J. Electrochem. Soc. 164 (2017) A6381-A6385.
[27] J.M. Tarascon, W.R. McKinnon, F. Coowar, T.N. Bowmer, G. Amatucci, D. Guyomard, J. Electrochem. Soc. 141 (1994) 1421-1431.
[28] J. Pires, A. Castets, L. Timperman, J. Santos-Peña, E. Dumont, S. Levasseur, C. Tessier, R. Dedryvère, M. Anouti, J. Power Sources 296 (2015) 413-425.

[29] X. Gao, Y.H. Ikuhara, C.A.J. Fisher, R. Huang, A. Kuwabara, H. Moriwake, K. Kohama, Y. Ikuhara, J. Mater. Chem. A 7 (2019) 8845-8854.
[30] D.J. Lee, D. Im, Y.-G. Ryu, S. Lee, J. Yoon, J. Lee, W. Choi, I. Jung, S. Lee, S.-G. Doo, J. Power Sources 243 (2013) 831-835.
[31] J. Pires, L. Timperman, A. Castets, J.S. Peña, E. Dumont, S. Levasseur, R. Dedryvère, C. Tessier, M. Anouti, RSC Adv. 5 (2015) 42088-42094.
[32] K. Abe, H. Yoshitake, T. Kitakura, T. Hattori, H. Wang, M. Yoshio, Electrochim. Acta 49 (2004) 4613-4622.
[33] M. He, C.-C. Su, C. Peebles, Z. Feng, J.G. Connell, C. Liao, Y. Wang, I.A. Shkrob, Z. Zhang, ACS Appl. Mater. Interfaces 8 (2016) 11450-11458.
[34] R. Sahore, A. Tornheim, C. Peebles, J. Garcia, F. Dogan, D.C. O'Hanlon, C. Liao, H. Iddir, Z. Zhang, J. Bareño, I. Bloom, J. Mater. Chem. A 6 (2018) 198-211.
[35] X. Xiao, Z. Liu, L. Baggetto, G. M. Veith, K. L. More, R. R. Unocic, Phys. Chem. Chem. Phys., 16 (2014) 10398-10402.
[36] K. Xu, Chem. Rev. 114 (2014) 11503-11618.
[37] Z. Zhang, L. Hu, H. Wu, W. Weng, M. Koh, P.C. Redfern, L.A. Curtiss, K. Amine, Energy Environ. Sci. 6 (2013) 1806-1810.
[38] C.L. Berhaut, P. Porion, L. Timperman, G. Schmidt, D. Lemordant, M. Anouti, Electrochim. Acta 180 (2015) 778-787.
[39] P. Porion, Y.R. Dougassa, C. Tessier, L. El Ouatani, J. Jacquemin, M. Anouti, Electrochim. Acta 114 (2013) 95-104.
[40] Y.R. Dougassa, J. Jacquemin, L. El Ouatani, C. Tessier, M. Anouti, J. Phys. Chem. B 118 (2014) 3973-3980.
[41] S. Amara, J. Toulc'Hoat, L. Timperman, A. Biller, H. Galiano, C. Marcel, M. Ledigabel, M. Anouti, ChemPhysChem 20 (2019) 581-594.
[42] F. Azeez, P.S. Fedkiw, J. Power Sources 195 (2010) 7627-7633.
[43] M. Doyle, T.F. Fuller, J. Newman, Electrochim. Acta 39 (1994) 2073-2081.
[44] K.M. Diederichsen, E.J. McShane, B.D. McCloskey, ACS Energy Lett. 2 (2017) 2563-2575.
[45] B. Flamme, G. Rodriguez Garcia, M. Weil, M. Haddad, P. Phansavath, V. Ratovelomanana-Vidal, A. Chagnes, Green Chem. 19 (2017) 1828-1849.
[46] A. Zaban, D. Aurbach, J. Power Sources 54 (1995) 289-295.
[47] T. Eriksson, A.M. Andersson, A.G. Bishop, C. Gejke, T. Gustafsson, J.O. Thomas, J. Electrochem. Soc. 149 (2002) A69-A78.

TOC

The combined effect of fluorinated additives (FEC and TTFP) or fluorinated co-solvent (TFEMC) have shown the best ability to reduce the fading of Graphite//$LiMn_2O_4$ cells cycled at high potential.